Atomic structure and friction of ultrathin films of KBr on Cu(100)

T. Filleter,* W. Paul, and R. Bennewitz
Department of Physics, McGill University, Montreal, Quebec H3A 2T8, Canada
(Received 30 August 2007; revised manuscript received 25 October 2007; published 25 January 2008)

The frictional properties of ultrathin films of KBr on a Cu(100) substrate have been studied on the atomic scale by means of friction force microscopy. Films as thin as two atomic layers support the sliding tip and exhibit atomic stick-slip friction similar to cleaved surfaces of bulk KBr. Steps on the film are prone to wear, while substrate steps overgrown by the film are found to be stable. The interpretation of these results is supported by a detailed analysis of the structure of the films by means of atomic-resolution noncontact force microscopy. The films are found to be compressively strained by 1.0 ± 0.2 %. They exhibit a regular superstructure originating from the interference of lattice constants at the substrate-film interface, which also causes a weak modulation of the frictional response. Monolayer films of KBr are subject to significant wear when imaged in contact-mode force microscopy. Noncontact imaging confirms that these monolayers are rich in defects.

DOI: 10.1103/PhysRevB.77.035430 PACS number(s): 68.35.Af, 62.20.Qp, 68.37.Ps

I. INTRODUCTION

The frictional properties of surfaces can be changed significantly by adsorbing molecularly thin films onto them. Self-assembled monolayers of organic molecules are one class of materials that have recently attracted wide attention both in fundamental tribology[1–3] and in applications to microelectromechanical systems.[4] Similarly, inorganic solid films with a thickness of a few atomic layers can change the frictional response of a surface. Macroscopic *in situ* experiments on well-defined films grown in vacuum have found friction reduction for ultrathin films of alkali and iron halides on iron surfaces[5,6] and for Ag on the Si(111) surface.[7]

Friction force microscopy is the tool of choice to study friction of such films with nanometer-scale resolution. It has been used to directly demonstrate the reduced friction on nanometer-thick WS_2 islands which develop as part of a transfer film in tungsten-sulfide-lubricated macroscopic contacts.[8] An example for the friction contrast of single layer films is a study of CaF and CaF_2 islands grown on a Si(111) surface.[9]

Friction force microscopy reveals more than only variations of the frictional response between different materials. Its sensitivity to mechanical processes at the atomic scale has also been used to explore fundamental phenomena of friction from a molecular perspective.[1] Even higher resolution can be achieved in the noncontact dynamic mode of force microscopy. It has been used to analyze the surface structure of insulating ultrathin films with atomic resolution, revealing the variation of interactions at different atomic sites.[10,11]

In this paper, we address the nanometer-scale frictional response of ultrathin films of KBr on a Cu(100) substrate surface. This system serves as a model toward understanding the fundamental tribological properties of engineering films such as $FeCl_2$ that form during extreme-pressure lubrication of iron.[5,6] In particular, this alkali halide and metal system has also been chosen because the atomic-scale frictional properties of both materials have been previously studied for their bulk surfaces.[12–17] Here, we demonstrate that the films are not only stable under contact-mode scanning but also yield atomic friction results. Using the full atomic-resolution capabilities of noncontact force microscopy, we characterize the film growth process and the film structure including structural defects which have an important influence on frictional response. After an introduction of the experimental methods, we present and discuss results for the film growth, the atomic structure of the film, and its frictional response. We then close with a summary connecting the atomic structure and friction results.

II. EXPERIMENTAL DETAILS

All experiments have been performed with an ultrahigh vacuum multimode atomic force microscope (AFM) operated at room temperature with a base pressure in the 10^{-11} mbar range.[18] Ultrathin films of KBr were deposited *in situ* on a freshly prepared Cu(100) single crystal substrate. The Cu sample was cleaned by repeated cycles of argon ion sputtering (1 keV) and annealing (725 K). Various thicknesses of KBr films, as measured by AFM imaging, were evaporated from a home-built Knudsen cell at a rate of $\sim$2.5 atomic layers/min onto the substrate kept at $\sim$350 K.

For this work, the multimode AFM has been operated in noncontact, Kelvin probe[19,20] and friction force modes. Two types of silicon cantilevers (Nanosensors) have been used for measurements. For noncontact and Kelvin probe measurements, stiff cantilevers with a backside coating of Al were used (f=160–180 kHz). In noncontact mode, topographic imaging was recorded using a constant amplitude. For friction force measurements, soft uncoated cantilevers were used (f=9–10 kHz, k_N=0.06–0.09 N/m, k_L=40–60 N/m). Normal and lateral force constants were individually calibrated in air using the Sader method.[21] For the noncontact cantilevers, argon ion sputtering was used to remove the native oxide layer from the tip. No such treatment was applied to the contact-mode cantilevers. For quantitative friction measurements, the normal load acting on the cantilever was determined with reference to the unbent cantilever. Positive and negative normal loads correspond to contact in the repulsive and attractive regimes, respectively. Average friction values

were determined from friction loops recorded in the forward and backward scan direction over the same position on the sample. The average friction force was calculated as half of the difference between the average lateral force in the forward and backward directions. Experimental results have been analyzed and converted into images by means of the WSXM software.[22]

III. EXPERIMENTAL RESULTS

A. Film growth

The first two atomic layers of KBr grow on Cu(100) in the form of large islands with side lengths of many hundreds of nanometers, smoothly overgrowing substrate steps. The "carpetlike" overgrowth of substrate steps has previously been observed for NaCl on Ge(100) (Ref. 23) and is attributed to the strong cohesion within the ionic films. The third and subsequent layers grow in the form of small rectangular islands with side lengths of a few tens of nanometers. The basic growth modes are schematically described in Fig. 1, the labels of which will be used to identify corresponding features throughout this paper.

The topography of the film growth is shown in the noncontact AFM image in Fig. 2. Large monolayer and bilayer films cover most of the surface. We have never observed isolated monolayer islands on the bare Cu substrate; the second layer always covers part of the large first-layer islands. Small rectangular islands of the third-layer cover the bilayer area of the film. No small rectangular islands have been observed on a monolayer film. This suggests that absorbed molecules are more mobile on the Cu(100) substrate and on monolayer films than on bilayer films. The kinetics of alkali halide growth are dominated by the motion of strongly bound diatomic molecules and are therefore generally discussed in terms of molecular diffusion.[24] Note that there is a decrease of island size and density close to the edges of bilayer areas. These step edges act as a trap for KBr molecules diffusing on the bilayer which then contribute to the growth of the second layer rather than forming islands of the third layer. The steps between monolayer and bilayer of KBr are typically less regular than the atomically straight edges of rectangular islands in the third layer [Fig. 2(b)]. The diffusion of molecules along island edges in conjunction with the reduced mobility on the bilayer produces islands with a minimum number of corner and kink sites.

The steps of the Cu(100) surface, clearly recognizable under the monolayer and the bilayer film, have a characteristic curved appearance, with kinks at sites where the step movement during surface preparation is pinned by impurities. Areas of the bare substrate surface can be identified by either the simultaneously recorded damping signal A_{exc} or by employing the Kelvin probe mode;[19,20] both provide a good material contrast on heterogeneous surfaces based on the variation of the work function for different materials.[25] Accurate height measurements of steps between bare Cu, monolayer, and bilayer areas of the KBr films have been achieved by compensation of the varying electrostatic interactions between those surface areas and the tip using Kelvin probe mode.

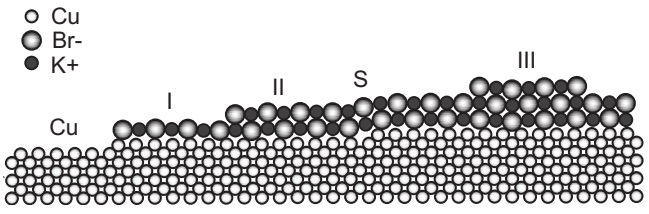

FIG. 1. Schematic representation of a stepped Cu(100) surface covered with an ultrathin film of KBr. (Cu) Bare Cu(100) substrate, (I) monolayer of KBr, (II) bilayer of KBr, (S) substrate step overgrown by the film in a carpetlike mode, and (III) third-layer island.

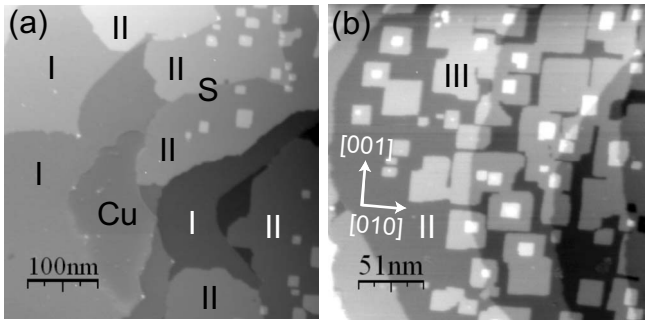

FIG. 2. (a) Noncontact AFM topography image of a Cu(100) surface covered with an ultrathin film of KBr. (b) Topography image showing detail of third- and fourth-layer island growth. Note that the regions are labeled with reference to Fig. 1.

From Kelvin probe measurements, the work function of the Cu substrate is found to be reduced by about 1.3 eV on the bilayer films. However, we find that a monolayer film of KBr reduces the work function only by about 1.1 eV. These numbers are only an approximation since quantitative Kelvin probe force microscopy requires a lateral extension of the structure under study which exceeds the tip radius,[20] a condition which is not fully satisfied for the areas of monolayer coverage we have measured. The work function difference between KBr and Cu(100) is higher but in the same range as that found for similar alkali halides on metal substrates.[25–27] A theoretical study by Olsson and Persson has predicted a difference in work function between a monolayer and a bilayer of NaCl on the strongly corrugated surface Cu(311).[28] The difference in work function between film layers was attributed to a stronger rumpling of the monolayer as compared to the bilayer film. A similar rumpling of the monolayer was predicted for the growth of NaCl on Cu(100), the substrate of this study. We will see in the next section that the atomic-scale structure of the KBr monolayer as observed by noncontact AFM is indeed less ordered than that of the bilayer.

Details of the growth of the small rectangular islands forming the third and fourth layers can be seen in Fig. 2(b). The KBr films generally grow with their ⟨100⟩ directions parallel to the ⟨100⟩ directions of the substrate surface which are indicated by arrows. This is evident from the orientation of the square islands and confirmed by low-energy electron diffraction (LEED) measurements and atomic-resolution imaging presented in the next section. The rectangular islands of the third layer have started to coalesce on the surface and

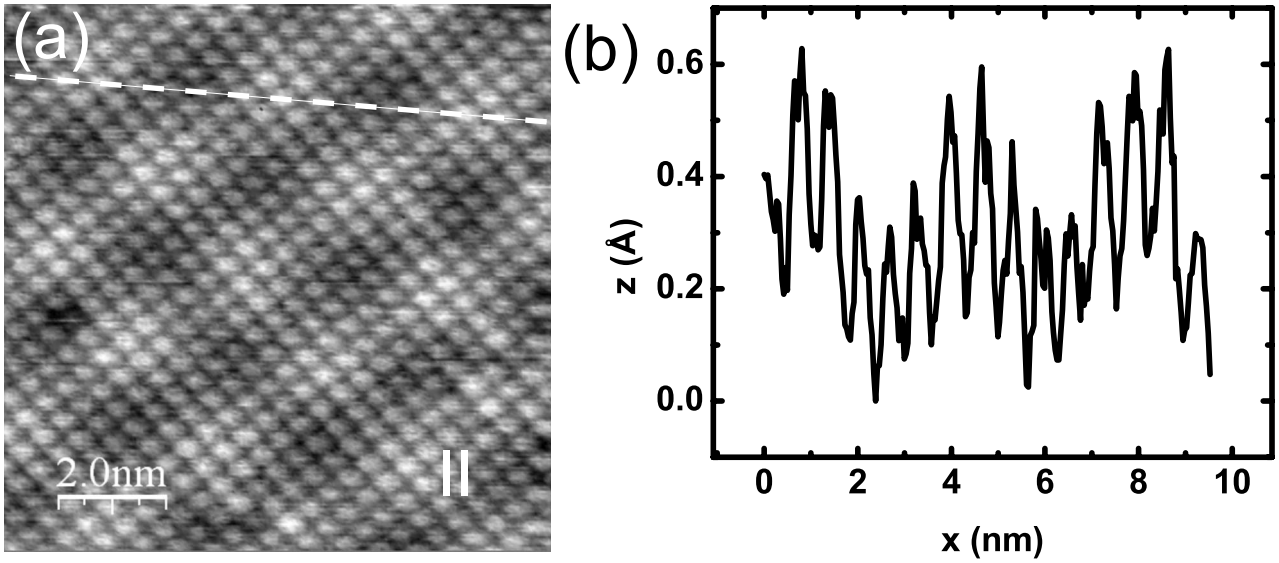

FIG. 3. (a) Noncontact AFM topography image of a bilayer of KBr showing both the superstructure and the atomic lattice. (b) Topography profile following the line indicated in (a). All AFM data in this paper is presented as measured with respect to drift in the slow vertical scan direction. The contribution from drift can be clearly observed in atomically resolved images such as in (a). Quantitative analysis has generally been performed using data recorded in the fast scan direction to avoid systematic errors caused by drift.

small fourth-layer islands reside in the center of the third layer, as shown in Fig. 2(b). This supports the conclusion that absorbed molecules have reduced mobility on films thicker than one monolayer. The nucleation of islands on the KBr bilayer seems to be largely homogeneous, since no defect sites enforce the nucleation of islands close to the edge of a bilayer terrace. On the other hand, a higher density of islands on top of underlying substrate steps [see Fig. 2(b)] indicates that either defects or strain in the bilayer above a substrate step provides the enhanced interaction or reduced mobility for a preferential nucleation.

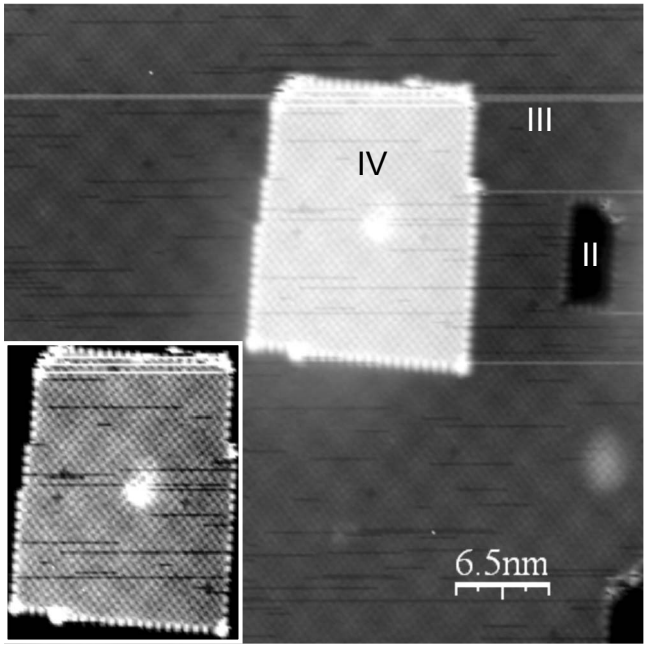

FIG. 4. Noncontact AFM topography image of a fourth-layer KBr island on top of a third-layer island. The inset shows the island in a different gray scale in order to highlight the appearance of the superstructure on the fourth-layer island.

The growth of alkali halide films on metal single crystals with straight nonpolar edges has been reported for many systems on both (100) and (111) substrate surfaces.[26,27,29–33] Growth of nanometer-size rectangular islands has previously been reported on both micrometer-size monolayer or bilayer islands[26,30,31,33] and directly on the substrate.[27,29,34,35] The actual growth mode may vary depending on substrate temperature and evaporation rates. For example, Repp *et al.* have observed that monolayer islands grow at lower substrate temperatures, whereas only bilayer islands grow at elevated temperatures.[33] The orientation of alkali halide films with respect to the underlying substrate lattice has been observed with perfect registry,[30,31,34] 45° rotation,[27] random orientation with certain preference toward the substrate orientation,[33] and random orientation or orientation at substrate step edges.[29,35] While the ionic bonds give the films a characteristic internal structure which includes the prevalence of straight nonpolar steps and the smooth overgrowth of substrate steps, their orientation seems to depend on very subtle details of the interactions at the substrate-film interface.

B. Atomic structure of the KBr films

Atomic-resolution images recorded by noncontact AFM are shown in Figs. 3 and 4. The atomic structure of the KBr film is imaged with only one of the ionic species protruding due to the modulation of the short-range electrostatic interaction by the differently charged ions. Step edges of islands in general and corner and kink sites, in particular, have a larger atomic corrugation reflecting the enhanced interactions at low-coordinated atomic sites.[10,32] Additional to the atomic structure of the film, a regular square-lattice superstructure is observed. Figures 3(a) and 4 show the superstructure on the second, third, and fourth layers of the KBr film. Detail of the

superstructure and a cross section of its topographic profile are shown in Fig. 3. The corrugation of the superstructure is of the order of 30 pm, very close to the observed corrugation of the atomic lattice. LEED measurements on the KBr films also show the presence of a superstructure through the appearance of satellite spots surrounding the KBr diffraction spots.

The bulk lattice spacing ratio of Cu and KBr is very close to 11:6 suggesting the development of a moiré pattern with a periodicity of 3.96 nm along the ⟨100⟩ directions. The experimentally observed superstructure was determined to be 3.54 ± 0.09 nm, very close to 5.5 unit cells of the KBr film. The observation of a smaller moiré pattern indicates that the KBr film is compressively strained, in this case by $1.0 \pm 0.2\%$. Direct measurements of the film lattice constant from atomically resolved images confirm this compression albeit with a larger error. Such a lateral contraction of an ultrathin alkali halide film is also in qualitative agreement with predictions of *ab initio* calculations.[28,29]

In conclusion, we assume that the superstructure originates in the interference of the lattice constants of a strained KBr film and of the substrate at the interface. Similar superstructures have been observed for NaCl on Cu(100),[36] NaCl on Ag(100),[27] and KBr on NaCl(100).[37] It is worth noting that the strain in the first bilayer does not allow a defect-free layer-by-layer growth of thicker films. The growth of the third layer in form of separated islands may be a consequence of the strain in the first bilayer.

We were not able to observe the atomic structure of monolayer films of KBr on Cu(100). Figure 5(a) shows a region of transition between a monolayer and a bilayer. High-resolution images were recorded on both in direct sequence. The atomically resolved image of the bilayer in Fig. 5(b) reveals the regular superstructure. The monolayer shown in Fig. 5(c), however, does not allow atomic resolution due to a high concentration of irregular defects in the film. This structural difference is also visible in the overview image in Fig. 5(a) where both layers are imaged simultaneously. While we do not know the exact nature of the defects in the monolayer film, it is interesting to note that Olsson and Persson have predicted less buckling for bilayer than for monolayer films for the similar system NaCl on Cu(100).[28]

The structure of the KBr films has also been investigated in regions where smooth growth occurs over monatomic steps of the Cu(100) surface. Such a step on a bare Cu(100) surface is shown in Fig. 6(a). The step edge appears fuzzy due to the high mobility of Cu atoms around the step edge at room temperature.[38] A step covered by a bilayer of KBr does not exhibit any visible fluctuations, and stable facets in the substrate step edge can be imaged over long time periods [see Fig. 6(b)]. The superstructure undergoes a phase shift of one-half of its period across the substrate step. This phase shift reflects the phase shift in the atomic lattice of the Cu substrate which is characteristic for adjacent (100) terraces of fcc metals separated by a monatomic step. In Fig. 6(b), the superstructure is rotated by about 14° with respect to the atomic lattice of the KBr film. Such a rotation suggests a 1.3° relative orientation between the KBr film and the Cu(100) substrate. The rotation is amplified by the moiré effect similar to the compression of the film. Figure 6(c) shows a high-resolution detail of a monatomic substrate step covered with a bilayer of KBr. The line profile of the topography across the step in Fig. 6(d) reveals that the expected step height of 0.18 nm is ascended by the KBr film within three of its unit cells. The shift of the moiré pattern at substrate steps and the perfectly crystalline overgrowth of the steps prove the strong cohesion within the film, while its slight rotation indicates that stress in the film close to substrate steps can affect the relative orientation of the film.

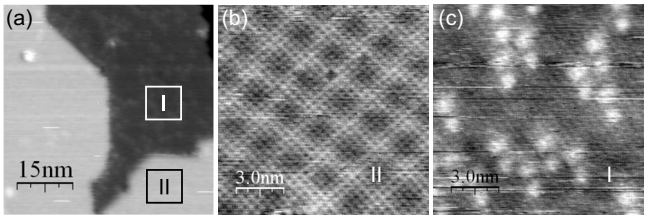

FIG. 5. (a) Noncontact AFM topography image of a monolayer to bilayer transition on a KBr film. (b) Atomically resolved region of bilayer KBr [black square in (a)]. (c) High-resolution image of a region of monolayer KBr showing a high number of defects [white square in (a)].

C. Friction measurements

Contact-mode force microscopy was used to investigate the frictional properties of the ultrathin KBr films. Figure 7(a) shows a typical topographic image of a KBr film recorded in contact mode. The characteristic structure of the film as described in Sec. III A with rectangular coalescing islands in the third layer and smaller rectangular islands of

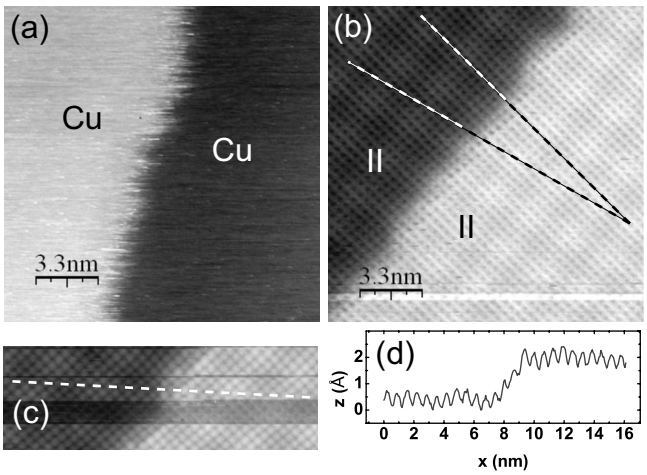

FIG. 6. (a) Noncontact AFM topography image of an area of bare Cu(100) with a monatomic step. (b) Topography image of a Cu(100) monatomic substrate step covered with a bilayer of KBr. The lines indicate both the phase shift in the superstructure across the step and the relative rotation of atomic lattice and superstructure. (c) High-resolution image of a Cu(100) monatomic step covered with a bilayer of KBr. (d) Line profile taken along the cross section indicated in (c) showing atomic corrugation across the step edge.

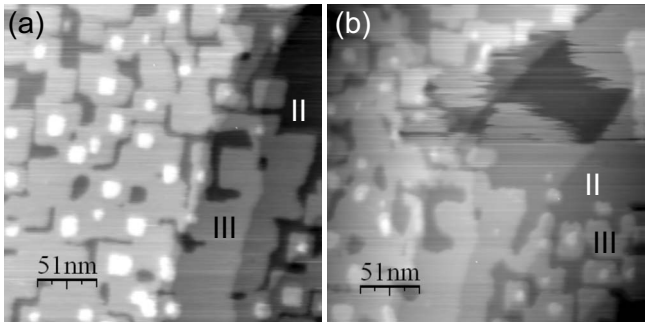

FIG. 7. (a) Typical contact AFM topography image of Cu(100) surface covered with an ultrathin film of KBr with up to fourth layer coverage. (b) Contact AFM image demonstrating significant wear initiated at the transition from a region of bare Cu to the KBr film. Both images are recorded at a constant normal load of −0.6 nN.

the fourth layer is fully reproduced by contact-mode imaging despite the multiatom contact and adhesion forces. Neither is the bilayer film worn off the Cu(100) substrate nor are the islands significantly altered by the scanning tip.

However, significant wear is typically found to occur at the transition from areas of bare Cu(100) surface to KBr films, as shown in Fig. 7(b). The fuzzy appearance of the film edge and the stripes starting at the edge indicate material being detached by the action of the tip and transferred over the surface. This wear at the edges of KBr films is significantly reduced for sharp tips with very low adhesion. An example for this situation is given in Fig. 8(a) which shows a contact-mode topography image of an area of the sample with bare Cu(100) and KBr film coverage up to the fourth layer.

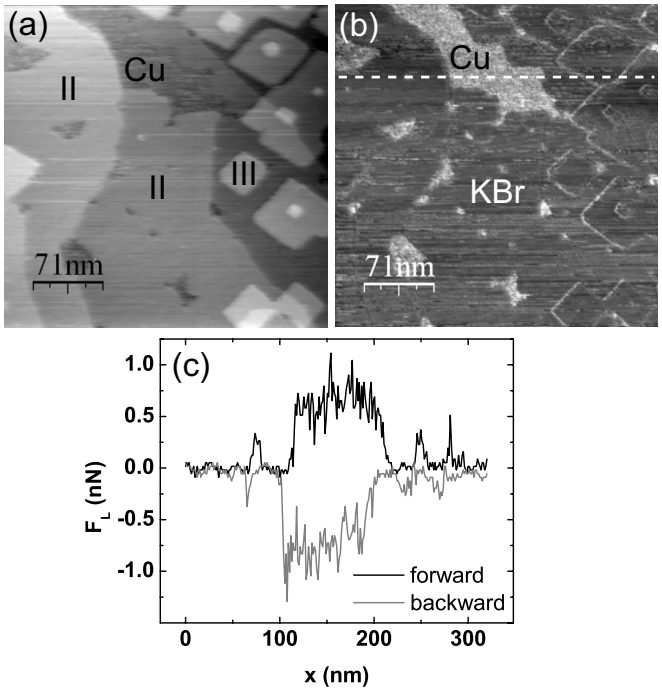

FIG. 8. (a) Contact AFM topography image of Cu(100) surface covered with an ultrathin film of KBr. (b) Simultaneously recorded lateral force map of the same area in the forward scan direction. (c) Line profile of the lateral force in both scan directions. The image was recorded at a constant normal load of −0.8 nN.

A strong friction contrast is observed between the KBr film and the Cu(100) substrate [see Fig. 8(b)]. The line profiles of the lateral force in Fig. 8(c) reveal that the average lateral force is significantly higher on the substrate (~0.7 nN) than on the film (<0.1 nN). The bilayer of KBr not only supports the tip while scanning in contact mode but it also reduces the frictional forces dramatically. No significant change in lateral force is observed between a bilayer of KBr and the third or fourth layer. However, increased lateral forces are detected at the step edges between different film layers, similar to observations at evaporation spirals on NaCl(100).[39] Systematic studies of friction on KBr monolayers have been hampered by wear at the transition between such monolayers and areas of bare Cu(100) substrate surface. As pointed out in Sec. III A, small patches of monolayer film are always found next to bare Cu(100) areas and no closed monolayer films could be grown. In the following, we will therefore describe the atomic-scale friction properties of bilayer films and subsequent island layers.

Figure 9(a) shows a lateral force map recorded in contact mode on the bilayer of a KBr film. The lateral force is found to follow the periodicity of the KBr lattice. This atomic stick-slip behavior is typical for friction force microscopy measurements on this scale for bulk KBr crystals. Here, we provide experimental evidence that bulklike atomic stick-slip is supported by films as thin as two atomic layers. Figure 9(c) shows a corresponding friction loop with the sawtooth characteristic and force values typical for bulk KBr(100).[13,17] We have found atomic stick-slip behavior also for bilayers of NaCl grown on Cu(100) (results not shown).

The slope of the sticking phase of the lateral force curve in Fig. 9(c) was used to calculate the lateral stiffness of the contact between the tip and sample according to Ref. 40. The lateral contact stiffness depends strongly on the contact size and hence will vary significantly between tips with differing apex radii. For different tips sliding on bilayer KBr films, we

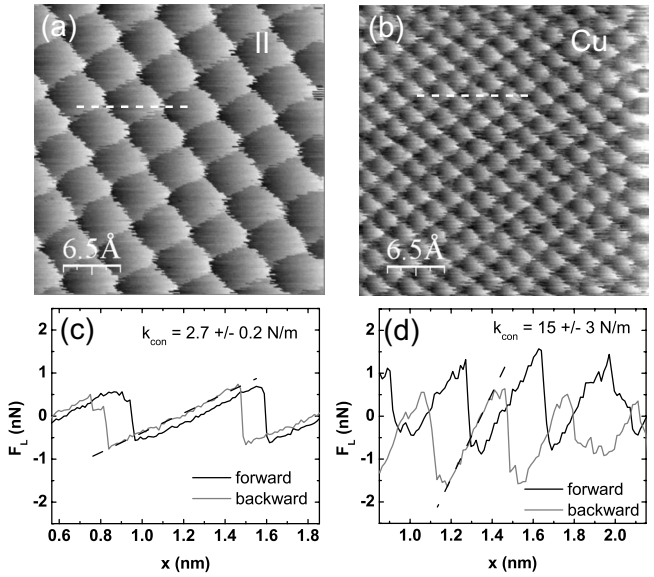

FIG. 9. (a) Lateral force map of a bilayer KBr film surface. (b) Lateral force map of a bare Cu(100) surface. [(c) and (d)] Lateral force line profiles for lines indicated in images (a) and (b), respectively.

found values between 1.1 and 2.7 N/m. This suggests that there is a systematic error associated with typical differences in tip radii on the order of a few N/m. The contact stiffness on the bilayer films are found to be in agreement with values for bulk KBr(100) of 1–5 N/m.[13,17] In summary, the bilayer films of KBr on Cu(100) exhibit an atomic stick-slip friction which is essentially the same as that found on bulk KBr(100) with respect to characteristic lateral force curves, typical force values, and lateral contact stiffness.

Figures 9(b) and 9(d) show a lateral force map and friction loop, respectively, for atomic stick-slip on the bare Cu(100) surface. The lateral force is found to regularly follow the periodicity of the Cu(100) surface lattice, without experimental difficulties reported previously.[16] Figures 9(a) and 9(b) have the same lateral scale and demonstrate the relative size of the Cu and KBr lattices with respect to one another. For the bare Cu(100) surface, the contact stiffness was found to be 15 ± 3 N/m. This value is significantly higher than the values stated above for the KBr films, but similar to a previously reported value of ~9 N/m for the Cu(111) surface.[15] It is remarkable that the atomic-scale frictional properties of the bilayer film are hardly influenced by the quite different properties of the substrate. The atomic structure of the tip apex and the surface layers dominate the possible influences of bulk elasticity or interface compliance.

The effect of the superstructure discussed in Sec. III B on the frictional properties of the films is summarized in Fig. 10. The lateral force shown in Fig. 10(a) exhibits a very weak periodic variation which is revealed in the Fourier transform shown in the inset. Two patterns with cubic symmetry are found, one with the periodicity of the KBr lattice and one corresponding to the superstructure. A line profile of the lateral force taken along the [010] direction of the lattice [Fig. 10(b)] shows a modulation in the amplitude of the stick-slip curve. The periodicity of the superstructure deviates from the 5.5 unit cells observed in Fig. 3 due to the rotation between superstructure and atomic lattice which is evident in the spatial frequency map in Fig. 10(a). A similar modulation of atomic friction has recently been observed on thin KBr films deposited on a NaCl(100) substrate.[41] It is difficult to judge whether the variation of the stick-slip amplitude is an effect of the topographic modulation or of a modulation of interactions at the interface between Cu(100) substrate and KBr film. A definite answer may require atomistic modeling of the system of substrate, film, and sliding tip.

Finally, we will discuss results regarding the frictional properties of KBr films at step sites. Figures 11(a)–11(c) present results for steps between a bilayer film and a third-layer KBr island, while Figs. 11(d) and 11(e) show details of the friction on a bilayer film growing across steps of the Cu(100) substrate.

The topographic contact-mode image of a third-layer island in Fig. 11(a) does not reveal any of the atomic details seen by noncontact-mode imaging in Figs. 3 or 4. Steps edges and, in particular, corner sites exhibit fuzzy stripe features indicating wear. The enhanced wear probability at the corner and edge sites can be directly explained using the noncontact image in Fig. 4. These sites of lower atomic coordination exhibit a strongly enhanced interaction with the tip as demonstrated by their protruding appearance. Such enhanced interaction makes the sites prone to wear off under the tip sliding in contact. Correspondingly, the lateral force maps in Figs. 11(b) and 11(c) exhibit regular stick-slip on the bilayer and on top of the island. However, the step edges appear rounded and the regular stick-slip pattern is disordered in a region of several unit cells around the step edges.

In contrast, the bilayer films overgrowing substrate steps are very stable and show little friction contrast at the step sites. The topographic image recorded in contact mode in Fig. 11(d) clearly reproduces the two underlying monatomic substrate steps. As already seen in Fig. 6(b), the substrate steps are stabilized by the bilayer film, preventing any wear from occurring that could be expected for the rather unstable monatomic substrate steps imaged in Fig. 6(a).[15] The simultaneously recorded lateral force map in Fig. 11(e) exhibits atomic stick-slip with a weak modulation revealing the film's superstructure. The underlying substrate steps cause only a

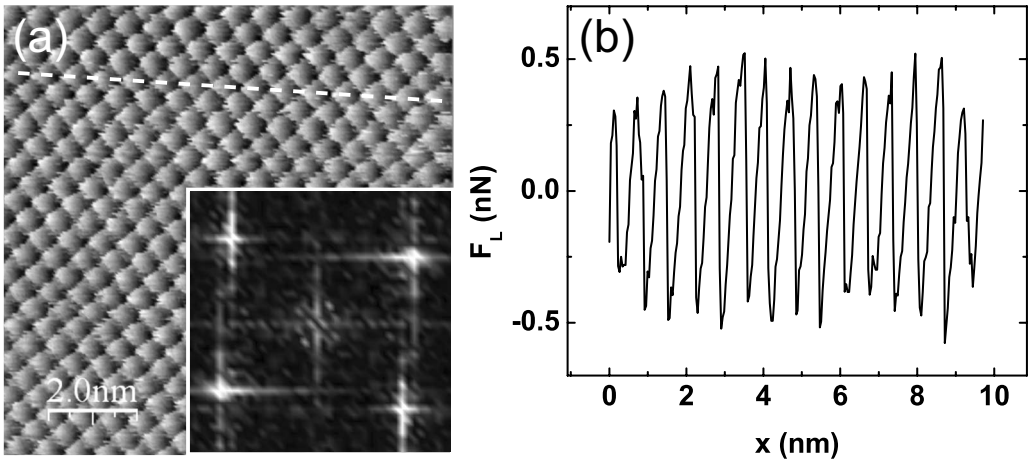

FIG. 10. (a) Lateral force map of the bilayer KBr film surface. The inset shows a spatial frequency map of the image with weak inner spots indicating the superstructure described in Sec. III B. (b) Lateral force line profile for the line indicated in image (a). Note the modulation in the amplitude of the lateral force.

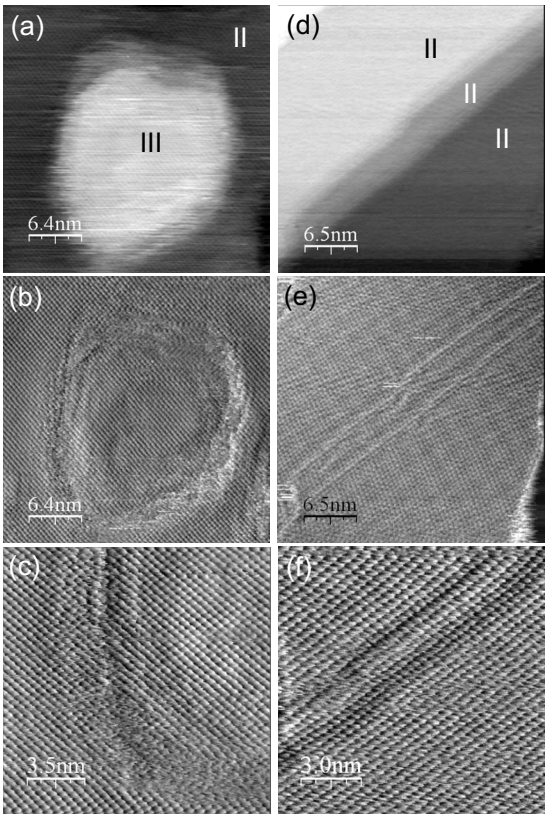

FIG. 11. Simultaneously recorded contact AFM images of (a) topography and (b) lateral force of a third-layer island. (c) High-resolution lateral force map of the bottom left corner of the island shown in (a). Simultaneously recorded contact AFM images of (a) topography and (b) lateral force on two adjacent Cu monatomic steps covered by a bilayer of KBr. Note the appearance of the superstructure as a modulation of the lateral force signal. (f) High-resolution lateral force map of a single Cu monatomic step covered with a bilayer of KBr.

small variation of the lateral force. The detailed view of a single monatomic step covered with a bilayer film in Fig. 11(f) demonstrates that the regular stick-slip pattern is not interrupted at the step site.

IV. CONCLUSION

Our friction force microscopy experiments demonstrate that KBr films as thin as two atomic layers on a Cu(100) substrate support the sliding tip in a way that is not distinguishable from bulk KBr crystals in terms of the appearance of atomic stick-slip, the typically observed force values, and the lateral contact stiffness. Lateral forces are dramatically reduced as compared to the metallic substrate. The only notable influence of the substrate on the frictional response of the films is a weak modulation of the amplitude of atomic stick-slip friction which resembles a superstructure arising from the mismatch between the lattice constants of the substrate and the strained films. This superstructure was analyzed in detail in noncontact-mode imaging with atomic resolution, revealing a compressive strain of $1.0 \pm 0.2\,\%$. Generally, the detailed analysis of film growth by means of high-resolution noncontact force microscopy provides essential information for the understanding of the frictional response of the thin film system. For example, the observation of a strongly enhanced interaction for step and kink sites at third-layer islands explains why these sites appear as nucleation sites for wear processes in friction force microscopy. On the other hand, noncontact-mode imaging demonstrates how the irregular and mobile monatomic substrate steps are smoothly covered, stratified, and stabilized by a continuous bilayer KBr film. The films provide a coherent basis for the sliding contact without appreciable friction contrast at the site of the substrate step. In summary, bilayer films of KBr act as efficient solid lubricant layers on Cu(100) substrates.

We have not been able to study the atomic-scale frictional response of monolayer films due to the occurrence of severe wear. Again, noncontact-mode imaging helps us understand that monolayer films have a high defect density and may not be structurally stable on Cu(100) substrates. Our results support the interpretation of macroscopic friction experiments on alkali halide films on an iron substrate by Gao *et al.*[5] Gao *et al.* reported a dramatic reduction in the friction on clean iron substrates by a factor of 4–5 for a variety of deposited halide films. The group concluded that a minimum friction coefficient is achieved as soon as a complete first layer of the film has formed on the substrate, as recently confirmed by deuterium titration experiments.[6] Our microscopic study confirms the importance of a closed film for the effective reduction of friction and protection against wear, which is achieved in form of bilayer films for our system.

ACKNOWLEDGMENTS

This work was supported by the Canada Foundation of Innovation and NSERC.

*filleter@physics.mcgill.ca

[1] *Nanotribology and Nanomechanics*, edited by B. Bhushan (Springer-Verlag, Berlin, 2005).
[2] R. Carpick, D. Sasaki, M. Marcus, M. Eriksson, and A. Burns, J. Phys.: Condens. Matter **16**, R679 (2004).
[3] G. J. Leggett, N. J. Brewer, and K. S. L. Chong, Phys. Chem. Chem. Phys. **7**, 1107 (2005).
[4] R. Maboudian and C. Carraro, Annu. Rev. Phys. Chem. **55**, 35 (2004).
[5] F. Gao, P. Kotvis, and W. Tysoe, Tribol. Lett. **15**, 327 (2003).
[6] O. Furlong, F. Gao, P. Kotvis, and W. Tysoe, Tribol. Int. (to be published).
[7] M. Goto, F. Honda, and M. Uemura, Wear **252**, 777 (2002).
[8] C. Drummond, N. Alcantar, J. Israelachvili, R. Tenne, and Y. Golan, Adv. Funct. Mater. **11**, 348 (2001).
[9] B. Müller, C. Wang, K. Hofmann, M. Bierkandt, C. Deiter, and J.

Wollschläger, Surf. Sci. **532-535**, 633 (2003).
[10] R. Bennewitz, A. S. Foster, L. N. Kantorovich, M. Bammerlin, C. Loppacher, S. Schär, M. Guggisberg, E. Meyer, and A. L. Shluger, Phys. Rev. B **62**, 2074 (2000).
[11] M. Heyde, G. Simon, H. Rust, and H.-J. Freund, Appl. Phys. Lett. **89**, 263107 (2006).
[12] F. Giessibl and G. Binnig, Ultramicroscopy **42-44**, 281 (1992).
[13] R. Lüthi, E. Meyer, M. Bammerlin, L. Howald, H. Haefke, T. Lehmann, C. Loppacher, and H.-J. Güntherodt, J. Vac. Sci. Technol. B **14**, 1280 (1996).
[14] R. Carpick, Q. Dai, D. Ogletree, and M. Salmeron, Tribol. Lett. **5**, 91 (1998).
[15] R. Bennewitz, T. Gyalog, M. Guggisberg, M. Bammerlin, E. Meyer, and H.-J. Güntherodt, Phys. Rev. B **60**, R11301 (1999).
[16] R. Bennewitz, E. Gnecco, T. Gyalog, and E. Meyer, Tribol. Lett. **10**, 51 (2001).
[17] U. Wyder, A. Baratoff, E. Meyer, L. Kantorovich, J. David, S. Maier, T. Filleter, and R. Bennewitz, J. Vac. Sci. Technol. B **25**, 1547 (2007).
[18] L. Howald, E. Meyer, R. Lüthi, H. Haefke, R. Overney, H. Rudin, and H.-J. Güntherodt, Appl. Phys. Lett. **63**, 117 (1993).
[19] M. Nonnenmacher, M. OBoyle, and H. K. Wickramasinghe, Appl. Phys. Lett. **58**, 2921 (1991).
[20] U. Zerweck, C. Loppacher, T. Otto, S. Grafstrom, and L. M. Eng, Phys. Rev. B **71**, 125424 (2005).
[21] C. Green, J. Lioe, H. Cleveland, R. Proksch, P. Mulvaney, and J. Sader, Rev. Sci. Instrum. **75**, 1988 (2004).
[22] I. Horcas, R. Fernandez, J. Gomez-Rodriguez, J. Colchero, J. Gomez-Herrero, and A. Baro, Rev. Sci. Instrum. **78**, 013705 (2007).
[23] C. Schwennicke, J. Schimmelpfennig, and H. Pfnür, Surf. Sci. **293**, 57 (1993).
[24] M. H. Yang and C. P. Flynn, Phys. Rev. Lett. **62**, 2476 (1989).
[25] R. Bennewitz, M. Bammerlin, M. Guggisberg, C. Loppacher, A. Baratoff, E. Meyer, and H.-J. Güntherodt, Surf. Interface Anal. **27**, 462 (1999).
[26] C. Loppacher, U. Zerweck, and L. Eng, Nanotechnology **15**, S9 (2004).
[27] M. Pivetta, F. Patthey, M. Stengel, A. Baldereschi, and W.-D. Schneider, Phys. Rev. B **72**, 115404 (2005).
[28] F. Olsson and M. Persson, Surf. Sci. **540**, 172 (2003).
[29] W. Hebenstreit, J. Redinger, Z. Horozova, M. Schmid, R. Podloucky, and P. Varga, Surf. Sci. **424**, L321 (1999).
[30] R. Bennewitz, V. Barwich, M. Bammerlin, M. Guggisberg, C. Loppacher, A. Baratoff, E. Meyer, and H.-J. Güntherodt, Surf. Sci. **438**, 289 (1999).
[31] J. Kolodziej, B. Such, P. Czuba, F. Krok, P. Piatkowski, and M. Szymonski, Surf. Sci. **506**, 12 (2002).
[32] R. Bennewitz, S. Schär, E. Gnecco, O. Pfeiffer, M. Bammerlin, and E. Meyer, Appl. Phys. A: Mater. Sci. Process. **78**, 837 (2004).
[33] J. Repp and G. Meyer, Appl. Phys. A: Mater. Sci. Process. **85**, 399406 (2006).
[34] K. Glöckler, M. Sokolowski, A. Soukopp, and E. Umbach, Phys. Rev. B **54**, 7705 (1996).
[35] L. Ramoino, M. Von Arx, S. Schintke, A. Baratoff, H.-J. Guntherodt, and T. Jung, Chem. Phys. Lett. **417**, 22 (2006).
[36] J. Repp, G. Meyer, S. M. Stojkovic, A. Gourdon, and C. Joachim, Phys. Rev. Lett. **94**, 026803 (2005).
[37] S. Maier, O. Pfeiffer, T. Glatzel, E. Meyer, T. Filleter, and R. Bennewitz, Phys. Rev. B **75**, 195408 (2007).
[38] M. Giesen, Prog. Surf. Sci. **68**, 1 (2001).
[39] E. Meyer, R. Lüthi, L. Howald, M. Bammerlin, M. Guggisberg, and H.-J. Güntherodt, J. Vac. Sci. Technol. B **14**, 1285 (1996).
[40] M. A. Lantz, S. J. O'Shea, A. C. F. Hoole, and M. E. Welland, Appl. Phys. Lett. **70**, 970 (1997).
[41] S. Maier, E. Gnecco, A. Baratoff, R. Bennewitz, and E. Meyer (unpublished).